iJRASET
International Journal For Research in Applied Science and Engineering Technology

INTERNATIONAL JOURNAL FOR RESEARCH

IN APPLIED SCIENCE & ENGINEERING TECHNOLOGY

Volume: 6 **Issue:** III **Month of publication:** March 2018

DOI: http://doi.org/10.22214/ijraset.2018.3067

www.ijraset.com

Call: 08813907089 | E-mail ID: ijraset@gmail.com

International Journal for Research in Applied Science & Engineering Technology (IJRASET)
ISSN: 2321-9653; IC Value: 45.98; SJ Impact Factor: 6.887
Volume 6 Issue III, March 2018- Available at www.ijraset.com

Effect of Ternary Additions X (Co, Rh, Ir) on Electronic Properties of TiPd Shape Memory Alloy: An ab-initio Study

Namitha Anna Koshi[1], Rita John[2]
[1, 2]*Department of Theoretical Physics, University of Madras Guindy Campus, Chennai - 600 025, India*

Abstract: ***The structural and electronic properties of TiPd-X (X = Co, Rh, Ir) alloys are studied using first principles calculations. The site preference of X impurities in TiPd is determined from the calculated formation energy. It is found that ternary additions X prefer Ti sublattice more than Pd sublattice for the composition considered. The densities of states (total, site and angular momentum decomposed) are plotted for both $Ti_{43.75}Pd_{50}X_{6.25}$ and $Ti_{50}Pd_{43.75}X_{6.25}$ series. The density of Ti d-states and localization effect of ternary additions at the Fermi level determines the phase stability of these compounds. Band structure calculations are consistent with the results of density of states. Fermi surface topology of $Ti_{43.75}Pd_{50}Co_{6.25}$ and $Ti_{43.75}Pd_{50}Ir_{6.25}$ are studied in detail. The electron density contour maps give a picture of the bonding situation in these alloys.***
Keywords: TiPd-X, Density functional theory, Electronic properties, Fermi surfaces, Band structure

I. INTRODUCTION

Shape memory alloys (SMA), a class of intermetallic compounds, have the ability to remember their original shape. The phenomenon that imparts this unique character to SMA is martensitic transformation. Martensitic transformations are displacive solid-to-solid structural phase transitions induced by thermo-mechanical treatment. The chemical composition of the parent and the product phases remain the same. Shape memory alloys which have gained popularity commercially are Ti-based and Cu-based alloys. Of which, TiNi enjoys special status due to its superior properties like corrosion to resistance, biocompatibility and high strength-to-weight ratio. TiNi are used in the fields of engineering (fastening devices, gas turbine engine parts) and medicine (cardiovascular stents, eyeglass frames, and orthodontic wires) [1]. Phase transition in shape memory alloys has an associated pre-martensitic transformation, which in most cases, is driven by the softening of a phonon. In TiNi, the origin of phonon softening (in the 1/3[110] TA_2 branch) has been traced to the strong electron-phonon interaction at the nesting areas of Fermi surface [2, 3]. In general, phonon anomalies and formation of charge-density-wave (CDW) are attributed to the Fermi surface instabilities. At the martensitic transformation temperature, TiNi transforms from the parent austenite cubic phase (B2 phase) to the product martensite monoclinic phase (B19' phase). Martensitic transformation temperature of TiNi is near room temperature which limits its application as a high temperature structural material. There is a need for SMA with transformation temperatures above room temperature to extend the area of applications to robotics, automotive and aerospace industries. TiPd and TiPt are the known binary Ti-based high temperature shape memory alloys. Both the alloys undergo martensitic transformation from the parent B2 phase to the product B19 phase which is orthorhombic. The addition of transition metal Ir to TiPt increases the martensitic transformation temperature further [4] whereas partial substitution of Pt with Co and Ru was reported to be effective in augmenting high temperature strength and shape memory properties of TiPt alloy [5]. There is no simple theory to predict the effect of ternary additions on shape memory alloys. Experimental work in this area is aimed at tailoring alloys (with ternary and quaternary additions) which have higher martensitic transformation temperatures. These engineered materials have poor mechanical and shape memory properties. Therefore, the experimentalists must be cautious in choosing impurities and also, it is expensive to try out various possible combinations. Ab-initio calculations play an important role in shortlisting possible candidates for experiments. In this report, we study the effect of ternary additions on the electronic properties of shape memory alloy TiPd. To the best of our knowledge, theoretical investigation on the effect of addition of X (Co, Rh, Ir) in B2 TiPd shape memory alloys have not been reported yet. In particular, this paper reports the electronic properties of TiPd alloyed with 6.25% of X (Co, Rh, Ir) using the full potential linearized augmented plane wave (FP-LAPW) method within the framework of density functional theory. The site preference of X impurities is studied based on the formation energy calculations. The paper is organized as follows. Section 2 gives the details of computation. The results and discussion are presented in Section 3 which is divided into two: structural properties and

electronic properties. In electronic properties subsection (3.2), density of states (DOS), band structure and Fermi surface, and charge density contours are discussed.

II. COMPUTATIONAL DETAILS

All the calculations reported here, are performed using the full potential linearized augmented plane wave (FP-LAPW) method which is based on density functional theory (DFT) as implemented in the WIEN2k code [6]. The LAPW basis is constructed by dividing the unit cell into i) muffin tin region - the region inside the sphere centered around each atom, ii) interstitial region - the remaining part outside the spheres. For the latter, the solutions are smoothly varying and plane wave like but in the former, they are rapidly varying and atomic like. Therefore each basis function is defined as a plane wave in the interstitial region, connected to linear combination of atomic like function in the muffin tin region. The generalized gradient approximation (GGA) parametrized by Perdew-Burke-Ernzerh of (PBE) [7] is used to treat exchange-correlation effects. An energy difference of -6.0 Ryd is set to separate the core and valence states. The cut-off parameter R_{mt} x k_{max} = 8.50 where R_{mt} is the smallest atomic radius and k_{max} is the magnitude of the largest k vector in the plane wave basis. The radii of muffin tin spheres for all constituent elements are in the range 2.39 - 2.50 a.u. Inside the atomic sphere, partial waves have the maximum l value of 10 (i.e. l_{max} and for the interstitial region, the charge density Fourier expansion parameter G_{max} is set to 12. A dense mesh of 3000 k-points for the unit cell and 900 k-points for supercells are used. Fermi surfaces are plotted with a denser mesh of 5000 k-points. The self-consistency is achieved up to E = 0.0001 Ryd and F = 1 mRyd/a.u.

III. RESULTS AND DISCUSSION

A. Structural Properties

The shape memory alloy TiPd crystallizes in the B2 phase (CsCl structure) at high temperatures. It has spacegroup Pm-3m (221). Fig. 1(a) shows the high temperature austenite phase of TiPd. In the present work, we add impurities X (Co, Rh, Ir) to equiatomic TiPd by constructing 2x2x2 supercells.

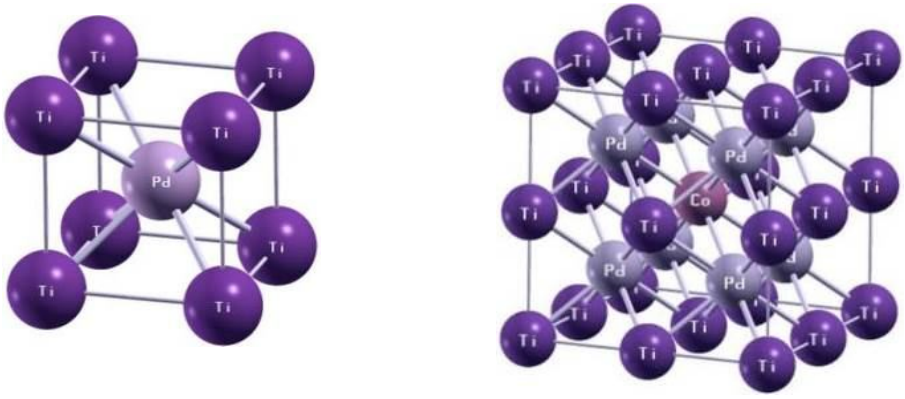

(a)
(b)
(c)
(d) (b)

Figure 1: Structure of (a) TiPd and (b) $Ti_{43.75}Pd_{50}Co_{6.25}$

The preferential site occupations of X additions are studied by substituting i) one Ti atom with X atom and ii) one Pd with X atom. For $Ti_{43.75}Pd_{50}X_{6.25}$ series, the resultant structure has five nonequivalent atoms and they are Ti1, Ti2, Ti3, X, and Pd with multiplicity 1, 3, 3, 1, and 8 respectively (hence, a total of 16 atoms per cell). Similarly, for $Ti_{50}Pd_{43.75}X_{6.25}$ series, the resultant structure has five nonequivalent atoms which are Ti, Pd1, Pd2, Pd3, and X with multiplicity 8, 1, 3, 3, and 1 respectively. For all the compounds investigated, total energies are calculated for different reduced and extended volumes and are fitted to the standard Murnaghan equation of state (EOS) [8]. Geometry minimization is performed using the PORT method (by L. D. Marks [9,10]) to find the equilibrium position of atoms, as implemented in WIEN2k code. Formation energy (FE) which is a measure of phase stability is calculated using the following equation:

FE = E_{tot} ($Ti_{50}Pd_{50-x}X_x$) – 50/100 E_{tot} (Ti) – (50-x)/100 E_{tot} (Pd) – x/100 E_{tot} (X) (1)Here E_{tot} ($Ti_{50}Pd_{50-x}X_x$) is the total energy per atom of $Ti_{50}Pd_{50-x}X_x$ cell. E_{tot} (Ti), E_{tot} (Pd) and E_{tot} (X) are the total energies per atom of the pure Ti, Pd, X unit cells respectively. From the analysis of formation energy, it is found that X impurities have a strong preference for Ti sublattice than Pd in TiPd-X alloys, as $Ti_{43.75}Pd_{50}X_{6.25}$ gives lower value of energies than $Ti_{50}Pd_{43.75}X_{6.25}$ (presented in Table 1). The theoretically determined lattice parameter (a) of TiPd using GGA is in excellent agreement with the experimental value of 6.009 bohr and the FP-LAPW result within the local density approximation is 5.883 bohr [11]. Since no other data are available for comparison of lattice parameter (a) and bulk modulus (K) of TiPd-X compounds, our results are considered as a prediction. For both the series, bulk modulus increases as we go down the group 8B (Co → Rh → Ir). The density of states at E_F [$N(E_F)$] and Sommerfeld coefficient (C_v/T) calculated for the respective compounds are shown in Table 1.

Table 1: Ground state properties of $Ti_{43.75}Pd_{50}X_{6.25}$ and $Ti_{50}Pd_{43.75}X_{6.25}$

Compound	a (bohr)	K (GPa)	FE (Ryd/atom)	$N(E_F)$ (states/ Ryd cell)	C_v/T (mJ/mol K^2)
TiPd	6.0005	153.43	-3785.3106	42.09	7.29
$Ti_{43.75}Pd_{50}Co_{6.25}$	11.9138	159.17	-3785.3228	375.04	64.98
$Ti_{50}Pd_{43.75}Co_{6.25}$	11.9376	160.85	-3312.1658	350.03	60.64
$Ti_{43.75}Pd_{50}Rh_{6.25}$	11.9670	162.24	-4233.9442	284.67	49.32
$Ti_{50}Pd_{43.75}Rh_{6.25}$	11.9836	160.98	-3760.7866	360.99	62.54
$Ti_{43.75}Pd_{50}Ir_{6.25}$	11.9728	168.10	-5459.5240	272.42	47.20
$Ti_{50}Pd_{43.75}Ir_{6.25}$	11.9808	165.52	-4986.3693	361.51	62.63

B. Electronic Properties

1) Density of States: The total density of states (DOS) of all compounds is studied. Fig.2 shows the DOS for $Ti_{43.75}Pd_{50}Co_{6.25}$ and $Ti_{43.75}Pd_{50}Ir_{6.25}$. It resembles the DOS of a bcc metal. The DOS curves have a double peak structure - two set of peaks separated by a pseudogap. Pseudogap is formed due to the hybridization between the constitutents of the intermetallics. The pseudogap separates the bonding and antibonding regions. In all the cases, the Fermi level E_F falls on the rising edge of one of the peaks in the antibonding region. In an intermetallic compound, there exists a relation between the position of Fermi level and stability of the compound. If the Fermi level E_F falls on the pseudogap, then the material is said to be more stable [12]. According to this criterion, the B2 phase compounds studied here are unstable. Within the rigid-band picture, the position of E_F in DOS is a method of determining stability of the compound. The B2 phase of TiPd is unstable. As per this model, adding impurities which increases the total number of electrons in the system will destabilize the B2 structure while those that decrease the number of electrons will stabilize it [13], which is the reason for adding X (Co, Rh, Ir) impurities to TiPd - B2, as X has less number of electrons than Pd. But our energy calculations demonstrate that X impurities prefer Ti sublattice than Pd. This cannot be explained by rigid-band picture, which is not sufficient to describe the effects of alloy substitution. The general features of the DOS of TiPd in B2 phase have already been reported [13-15]. The total DOS at E_F [$N(E_F)$], for all compounds are listed in Table 1. Lower the value of $N(E_F)$, higher the stability. From the $N(E_F)$ values, $Ti_{43.75}Pd_{50}Ir_{6.25}$ has better stability among the three $Ti_{43.75}Pd_{50}X_{6.25}$ compounds and $Ti_{50}Pd_{43.75}Co_{6.25}$ among the $Ti_{50}Pd_{43.75}X_{6.25}$ series. The higher stability of $Ti_{43.75}Pd_{50}Ir_{6.25}$ is consistent with the energy calculations but not for $Ti_{50}Pd_{43.75}Co_{6.25}$. Similar disparity has been reported by J. Cai et al. [16] in their studies on the phase stability of B2 Ti-based binary shape memory alloys.

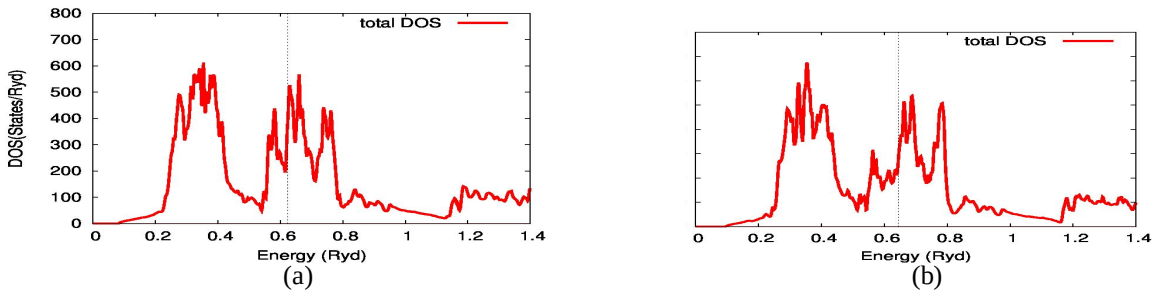

Figure 2: Total DOS for B2 phase (a) $Ti_{43.75}Pd_{50}Co_{6.25}$ and (b) $Ti_{43.75}Pd_{50}Ir_{6.25}$. E_F is represented by the black dotted line.

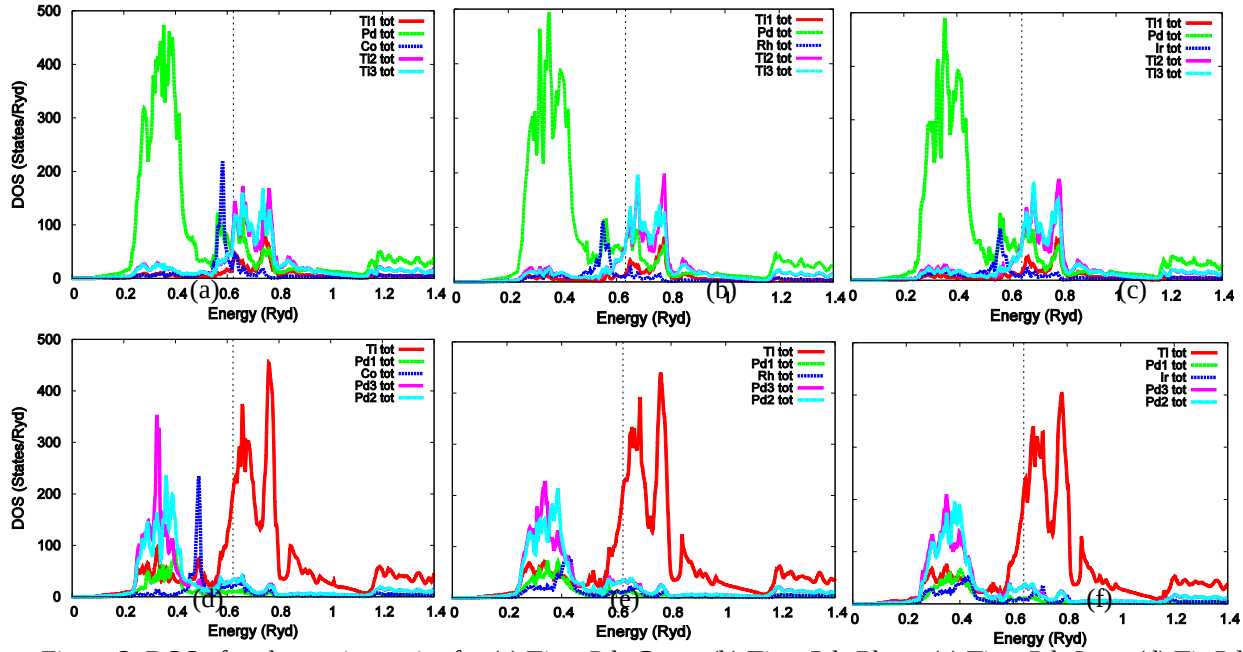

Figure 3: DOS of each atomic species for (a) $Ti_{43.75}Pd_{50}Co_{6.25}$, (b) $Ti_{43.75}Pd_{50}Rh_{6.25}$, (c) $Ti_{43.75}Pd_{50}Ir_{6.25}$, (d) $Ti_{50}Pd_{43.75}Co_{6.25}$, (e) $Ti_{50}Pd_{43.75}Rh_{6.25}$, (f) $Ti_{50}Pd_{43.75}Ir_{6.25}$. E_F is represented by the black dotted line.

A better understanding of the changes in electronic structure can be obtained by decomposing the DOS into site and angular momentum contributions. Fig.3 gives the total atomic DOS of each species in the compound. From Figs.3 (a)-(c), we conclude that the bonding region is dominated by Pd states in $Ti_{43.75}Pd_{50}X_{6.25}$ whereas antibonding region is an admixture of X, Pd, and Ti states. Of which, major contribution is from Ti states (or Ti states have more dominance over other constituents in the antibonding region). For $Ti_{50}Pd_{43.75}X_{6.25}$ [Figs. 3(d)-(f)], the bonding region is composed of Ti, Pd, and X states with the major contribution from Pd. However, the antibonding region is dominated by Ti states. In the $Ti_{50}Pd_{43.75}X_{6.25}$ series, the major contribution at E_F is from Ti atoms whereas in the $Ti_{43.75}Pd_{50}X_{6.25}$ series, both Pd and Ti atoms contribute.

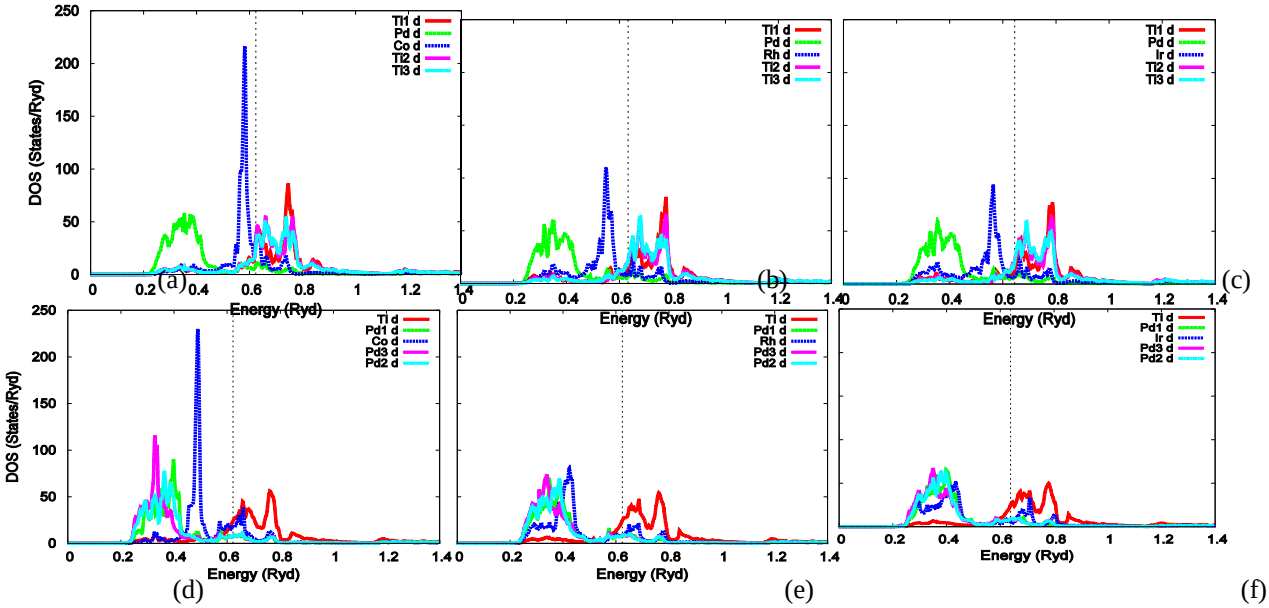

Figure 4: Density of d states of (a) $Ti_{43.75}Pd_{50}Co_{6.25}$, (b) $Ti_{43.75}Pd_{50}Rh_{6.25}$, (c) $Ti_{43.75}Pd_{50}Ir_{6.25}$, (d) $Ti_{50}Pd_{43.75}Co_{6.25}$, (e) $Ti_{50}Pd_{43.75}Rh_{6.25}$, (f) $Ti_{50}Pd_{43.75}Ir_{6.25}$ for the B2 phase. E_F is represented by the black dotted line.

In $Ti_{43.75}Pd_{50}X_{6.25}$ series, X has a peak between 0.5 Ryd and E_F. The peak decreases as we go down the group (i.e. Co→Rh→Ir) and it shifts slightly towards lower energies. In $Ti_{50}Pd_{43.75}X_{6.25}$ series, Co shows a significant peak around 0.5 Ryd which smears out and mixes with other constituents in the case of Rh and Ir substitution. Here the shift of X peaks is more pronounced in $Ti_{50}Pd_{43.75}Rh_{6.25}$ and $Ti_{50}Pd_{43.75}Ir_{6.25}$ than in $Ti_{43.75}Pd_{50}X_{6.25}$ series. Fig.4 gives the contribution of d-electrons (d-DOS) of the constituent elements of the compounds. In the $Ti_{50}Pd_{43.75}X_{6.25}$ series, as X goes from Co→Rh→Ir, there is a decrease in DOS (d-states) in the energy range 0.2-0.5 Ryd (bonding region). The Ti contribution (d-states) in antibonding region of $Ti_{50}Pd_{43.75}X_{6.25}$ series remains almost same. It is observed that d-states of X atoms are responsible for the peak in the bonding region of the corresponding compounds. For the impurity Co, the peak in the bonding region is more prominent in both the compositions. There is strong d-d hybridization between Ti and Co in $Ti_{43.75}Pd_{50}Co_{6.25}$ [Fig.4 (a)] at E_F. The splitting of degenerate d-orbitals into e_g (doublet) and t_{2g} (triplet) is a characteristic of B2 phase compounds [17]. The e_g (d_z^2, $d_{x^2-y^2}$) orbitals have higher energy than the t_{2g} (d_{xy}, d_{yz}, d_{zx}) orbitals for structures with octahedral point group, O_h. From the analysis of m-decomposed DOS of the compounds it is found that in the $Ti_{43.75}Pd_{50}X_{6.25}$ series, X peak in the bonding region corresponds to the d-e_g and d-t_{2g} states with a small majority from d-e_g. But in $Ti_{50}Pd_{43.75}X_{6.25}$ series, the d-e_g contribution towards X peak is very small and it is d-t_{2g} which dominates. At Fermi level E_F, total d contribution of Ti dominates in all the compositions, followed by Pd and X d-states (Fig.5). With reference to E_F, Pd states are bound hence the active Ti states dominate irrespective of impurity X. As we go down the group (Co→Rh →Ir), the contribution of impurity atom X at E_F decreases as shown in column graph (Fig.5). The s and p states of the constituents of compounds do not contribute much towards the structure of density of states. As expected, p-d hybridization is not found in these compounds. The present study shows that Rh and Ir belonging to the 4d and 5d series respectively, have similar behaviour, which differs significantly from Co belonging to 3d series. This reinforces the fact that 4d and 5d metals have properties closer to each other.

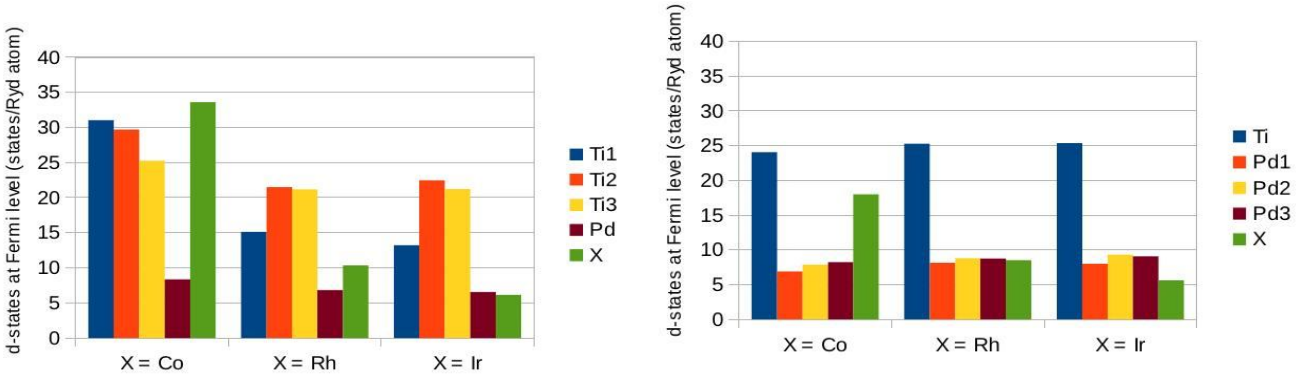

(a) (b)

Figure 5: Density of d-states at Fermi level, E_F for (a) $Ti_{43.75}Pd_{50}X_{6.25}$ and (b) $Ti_{50}Pd_{43.75}X_{6.25}$. In Fig.(a), Ti1, Ti2, and Ti3 represent the three nonequivalent Ti atoms in the $Ti_{43.75}Pd_{50}X_{6.25}$ series and in Fig.(b), Pd1, Pd2, and Pd3 represent the three nonequivalent Pd atoms in $Ti_{50}Pd_{43.75}X_{6.25}$ series.

It is known that the stability of Ti-based B2 phase compounds are determined by the Ti d-states at Fermi level. In Ti-based compounds, higher stability corresponds to a lower Ti d DOS value at the Fermi level [18]. The higher stability of $Ti_{43.75}Pd_{50}X_{6.25}$ can be attributed to the decrease in the density of d states of Ti and X at Fermi level with increasing atomic number of X impurities. The latter is due to the localization effect of transition metals (X) observed along the group. Though localization effect of X is more pronounced in $Ti_{50}Pd_{43.75}X_{6.25}$ series, the density of d-states of Ti at Fermi level remains same, hence lesser stability. Localization of d-states of transition metals both within the same period and along the group in Ti-based B2 compounds have been reported [19, 20].

2) Band structure and Fermi surface: The energy dispersion relation (E versus k) for TiPd and $Ti_{43.75}Pd_{50}Co_{6.25}$ are plotted in Figs.6 and 7 respectively. The chosen k-path for the cubic phase is Γ-X-M Γ -R-M-X-R [21]. It is clear that the band structure calculations are consistent with the results of DOS. From the band structure of $Ti_{43.75}Pd_{50}Co_{6.25}$, it is evident that the region above Fermi level are mostly occupied by Ti d-bands followed by small contribution from Co d-bands and the region below Fermi level by Pd and Co d-bands. Just below Fermi level (around 0.6 Ryd), Co d-states contribute largely which corresponds to the peak in the DOS curve of $Ti_{43.75}Pd_{50}Co_{6.25}$ [Fig.4(a)]. Lower lying s and p-states of the constituent elements do not contribute much at Fermi level and hence are not actively involved in determining the properties of these materials. Similar features are observed in the band structure of

$Ti_{43.75}Pd_{50}Ir_{6.25}$with the Ir bands slightly shifted towards lower energy region. Band structure of $Ti_{43.75}Pd_{50}Rh_{6.25}$ is generic in nature with that of $Ti_{43.75}Pd_{50}Ir_{6.25}$.

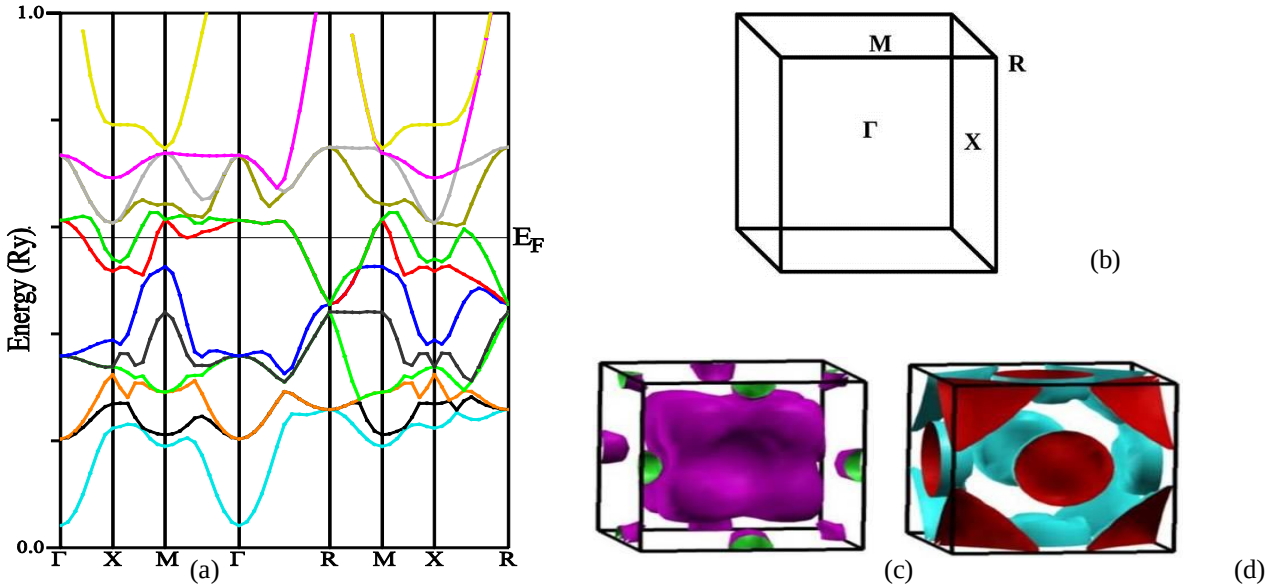

Figure 6: Band structure of TiPd, (b) Brillouin zone of a cubic crystal with high symmetry k-points, (c) Fermi surface of TiPd due to band 14 and (d) Fermi surface of TiPd due to band 15.

Fermi surface (FS) is a surface in reciprocal space that separates the occupied electron orbitals from the unoccupied. It is a constant energy surface. The study of Fermi surface topology is significant in shape memory alloys as Fermi surface nesting and strong electron-phonon coupling are found in conventional systems like Ni Al and Ni Ti [22]. The Fermi surfaces of TiPd - B2 are shown in Fig.6 (c) and (d). FS are plotted for the bands which cross the Fermi level. In TiPd, two bands cross the Fermi level and hence two Fermi sheets. The shapes of the Fermi surfaces obtained are consistent with the result of Hua Li et al. [23]. The sheet from band 14 (red) has a hole-like character whereas the sheet from band 15 (green) has an electron-like character. Fermi sheet arising from band 14 is a rounded cube centered at Γ and has a small hole pocket at M. Band 15 has electron pockets at X and R. The electron and hole pockets in relation to Fermi surfaces are discussed in [24]. The energy ranges for bands 14 and 15 are 0.470-0.612 Ryd and 0.470-0.628 Ryd respectively.

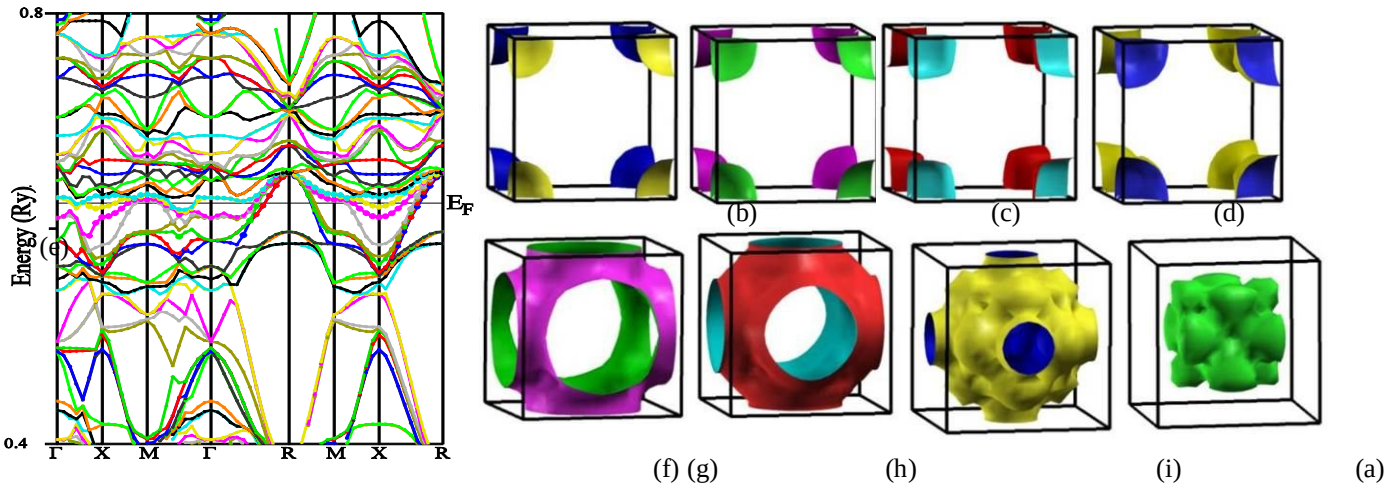

Figure 7: Band structure of (a) $Ti_{43.75}Pd_{50}Co_{6.25}$ - eight bands that cross the Fermi level (for clarity, smaller energy range is used). Fermi surfaces of (b) band 109, (c) band 110, (d) band 111, (e) band 112, (f) band 113, (g) band 114, (h) band 115 and (i) band 116.

Here $Ti_{43.75}Pd_{50}X_{6.25}$ series being energetically more stable are considered. The Fermi surfaces of $Ti_{43.75}Pd_{50}Co_{6.25}$ is shown in Figs.7 (a). In the $Ti_{43.75}Pd_{50}X_{6.25}$ series, eight bands cross the Fermi level which give rise to eight Fermi sheets. For $Ti_{43.75}Pd_{50}Co_{6.25}$, bands 109 (blue), 110 (red), 111 (green), and 112 (yellowish brown) have hole pockets at R and the corresponding FS are shown in Figs.7 (b)-(e). The hole surfaces are centered at R in these Fermi sheets. FS of bands 113, 114, and 115 (grey, majenta, and yellow) have mixed character [Figs.7 (f)-(h)] and the appropriate electron and hole pockets are also found in band structure [Fig.7 (a)]. Some of the pockets are not exactly at the high symmetry points but between them, for e.g., band 115 (yellow) has an electron pocket in the M-Γ direction. This along with the mixed character renders complicated shape to Fermi surface. Fermi surface arising from band 116 (cyan) have electron character [Fig.7 (i)]. The bands in the ascending order have energy ranges as 0.560-0.649 Ryd, 0.560-0.649 Ryd, 0.567-0.650 Ryd, 0.572-0.650 Ryd, 0.580-0.650 Ryd, 0.593-0.651 Ryd, 0.616-0.652 Ryd and 0.617-0.652 Ryd. The shape of Fermi surfaces of $Ti_{43.75}Pd_{50}Rh_{6.25}$and $Ti_{43.75}Pd_{50}Ir_{6.25}$ are identical, which indicate the similarity in the behaviour of 4d and 5d transition metals.

3) Electron density contour

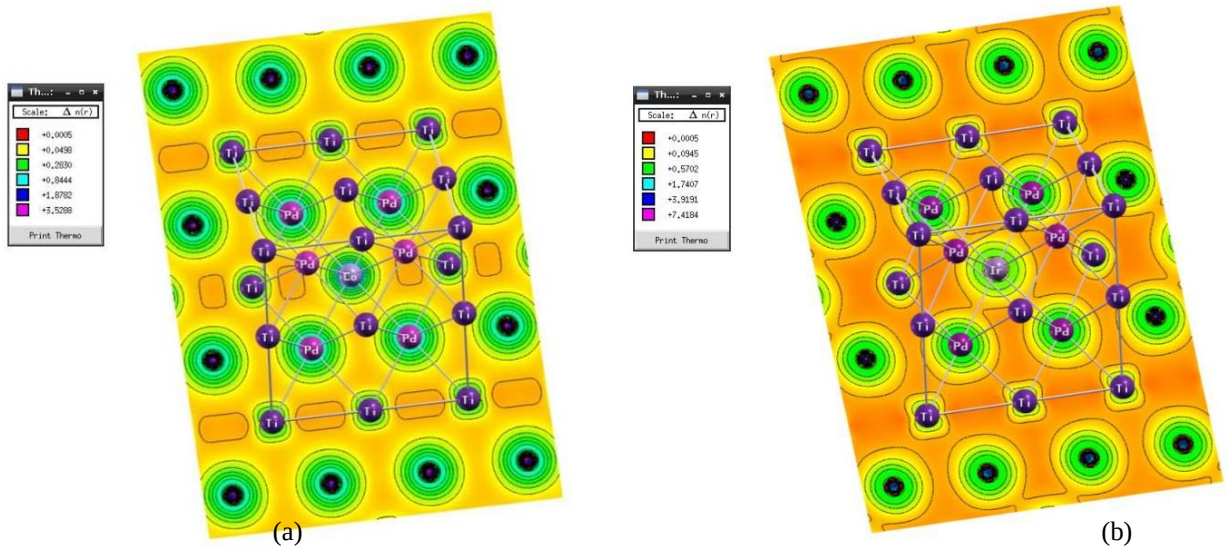

(a) (b)

Figure 8: Electron density contour of (a) $Ti_{43.75}Pd_{50}Co_{6.25}$ and (b) $Ti_{43.75}Pd_{50}Ir_{6.25}$

The electron density contours of $Ti_{43.75}Pd_{50}Co_{6.25}$ and $Ti_{43.75}Pd_{50}Ir_{6.25}$ for the (110) plane inscribed in the cell are plotted in Fig.8. As shown in Fig.8 (a), Co and Pd atoms have spherical electron density. Ti atoms at the face center of the cell also have spherical electron density, whereas those at the corners and along the edges of the cell have slightly distorted shape. The bonding nature seems to be metallic and no directional bonds are seen in the electron density plot. In $Ti_{43.75}Pd_{50}Ir_{6.25}$, there is small directional bonding between the nearest neighbor atoms Pd and Ir as seen in Fig.8 (b). Also, the electron density of Ti atoms at the face center is not spherical. But the electron densities of Ti atoms at the corners and edges of the cell have similar shape. In Ti-based B2 binary compounds, the decreasing stability of CsCl structure along the period is explained by the decreasing strength of covalent bonds between the nearest neighbours [17]. Here, the greater stability of $Ti_{43.75}Pd_{50}Ir_{6.25}$, to an extent, could be accounted for with the increasing directional bonding observed from Co→Rh→Ir.

IV. CONCLUSION

In conclusion, we have investigated the structural and electronic properties of TiPd-X alloys for the substitution of one host atom with impurity X (Co, Rh, Ir) using the FP-LAPW method implemented in WIEN2k code with PBE-GGA as the exchange-correlation potential. From the energy calculations, it was found that X impurities have strong preference for Ti sublattice than Pd sublattice. The ground state properties such as bulk modulus, density of states at E_F [$N(E_F)$], and Sommerfeld coefficient were computed. In the DOS calculations, we observed a peak of X impurities in the bonding region. The peak decreases as we go along group 8B (Co→ Rh→Ir). The stability of these compounds was determined by the density of Ti-d states at E_F and the localization of X impurities. The band structures and Fermi surfaces of the more stable series $Ti_{43.75}Pd_{50}X_{6.25}$ were plotted. From the electron

density contour plots, we conclude that the greater stability of $Ti_{43.75}Pd_{50}Ir_{6.25}$ is due to the directional bonding observed between nearest neighbours Pd and Ir.

V. ACKNOWLEDGEMENT

One of the authors N. A. K. acknowledges the Department of Science and Technology (DST), Government of India for the INSPIRE Fellowship. The authors express their sincere gratitude to Mr. T. Samuel, Application Programmer, Department of Theoretical Physics, University of Madras for his timely support during this work.

REFERENCES

[1] Morgan N B, 2004, Mater. Sci. Eng. A 378 16
[2] Shapiro S M, Noda Y, Fujii Y and Yamada Y, 1984, Phys. Rev. B 30 8 4314
[3] Satija S K, Shapiro S M, Salamon M B and Wayman C M, 1984, Phys. Rev. B 29 11 6031
[4] Yamabe-Mitarai Y, Hara T, Miura S and Hosoda H, 2006, Mater. Trans. 47 3 650
[5] Wadood A and Yamabe-Mitarai Y, 2014, Mater. Sci. Eng. A 601 106
[6] Blaha P, Schwarz K, Madsen G K H, Kvasnicka D and Luitz J, 2001, WIEN2k, An Augmented Plane Wave + Local Orbitals Program for Calculating Crystal Properties, Karlheinz Schwarz. Techn. Universität Wien, Austria, ISBN 3-9501031-1-2
[7] Perdew J P, Burke K, and Ernzerhof M, 1996, Phys. Rev. Lett. 77 18 3865
[8] Murnaghan F D, 1944, Proc. Nat. Acad. Sci. 30 9 244
[9] Marks L D and Luke R, 2008, Phys. Rev. B 78 075114
[10] Marks L D, 2013, J. Chem. Theory Comput. 9 2786
[11] Huang X, Rabe K M and Ackland G J, 2003, Phys. Rev. B 67 024101
[12] Ravindran P, Subramoniam G and Asokamani R, 1996, Phys. Rev. B 53 3 1129
[13] Ye Y Y, Chan C T and Ho K M, 1997, Phys. Rev. B 56 7 3678
[14] Liu H J and Ye Y Y, 1998, Solid State Commun. 106 4 197
[15] Bihlmayer G, Eibler R and Neckel A, 1993, J. Phys.:Condens. Matter 5 5083
[16] Cai J, Wang D S, Liu S J, Duan S Q and Ma B K, 1999, Phys. Rev. B 60 23 15691
[17] Eibler R, Redinger J and Neckel A, 1987, J. Phys. F: Met. Phys. 17 1533
[18] Tan C, Cai W and Zhu J, 2006, Phys. Stat. Sol. (b) 243 11 R69
[19] Shabalovskaya S, Narmonev A, Ivanova O and Dementjev A, 1993, Phys. Rev. B 48 18 13296
[20] John R and Ruben H, 2011, Materials Sciences and Applications 2 1355
[21] Setyawan W and Curtarolo S, 2010, Comput. Mater. Sci. 49 2 299
[22] Gruner M E, Adeagbo W A, Zayak A T, Hucht A and Entel P, 2010, Phys. Rev. B 81 064109
[23] Li H, Tokii M and Matsumoto M ,2012, J. Phys.:Condens. Matter 24 015501
[24] Fatima B, Chouhan S S, Acharya N and Sanyal S P, 2014,Comput. Mater. Sci. 89 205
[25] Opahle I, Koepernik K, Nitzsche U and Richter M, 2009, Appl. Phys. Lett. 94 072508

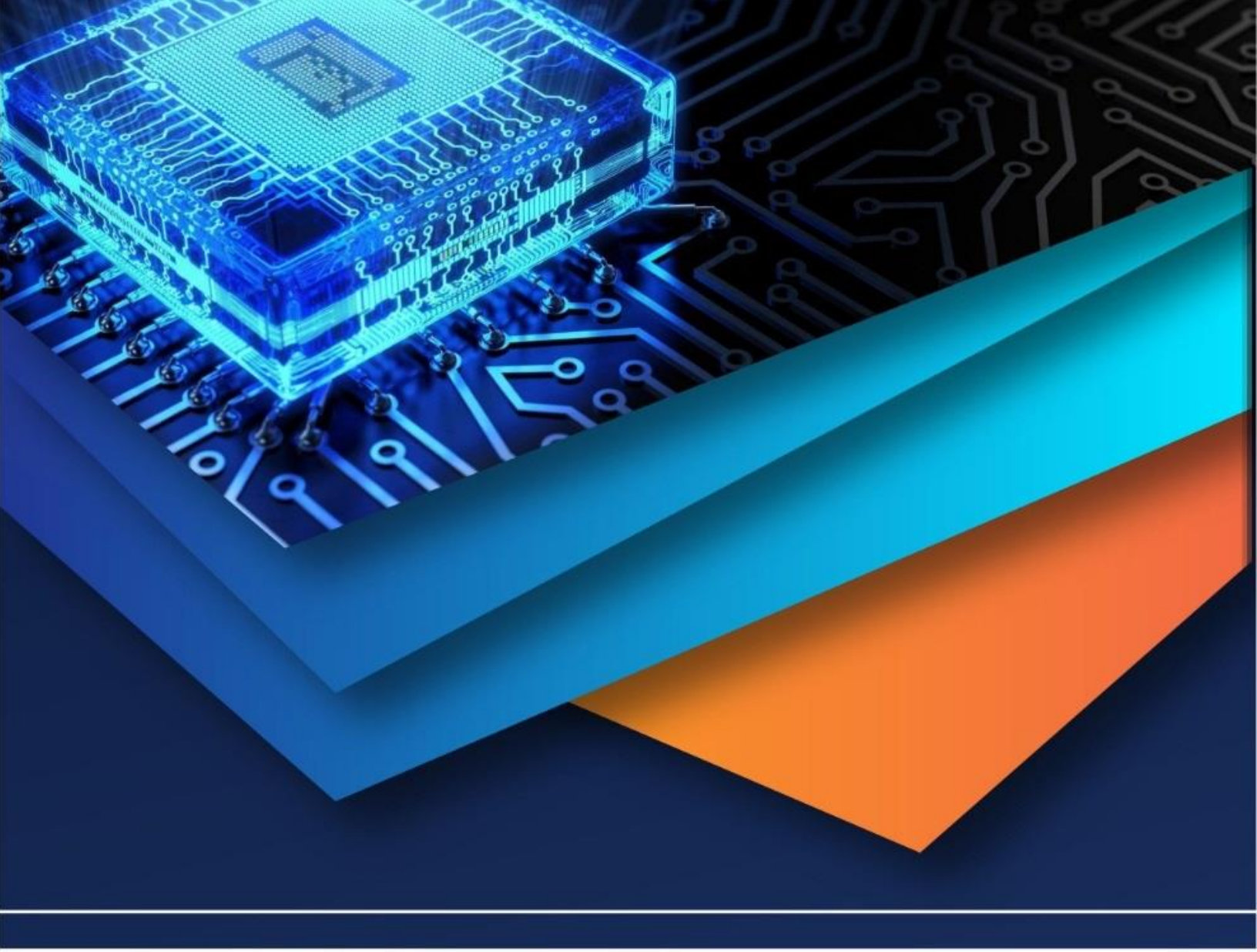

10.22214/IJRASET

45.98

IMPACT FACTOR: 7.129

IMPACT FACTOR: 7.429

INTERNATIONAL JOURNAL FOR RESEARCH

IN APPLIED SCIENCE & ENGINEERING TECHNOLOGY